Published in final edited form as:
Glia. 2012 July ; 60(7): 1117–1129. doi:10.1002/glia.22339.

ICV-Transplanted Human Glial Precursor Cells Are Short-Lived Yet Exert Immunomodulatory Effects in Mice with EAE

HEECHUL KIM[1,2], **PIOTR WALCZAK**[1,2], **NASER MUJA**[1,2], **JAMES T. CAMPANELLI**[3], and **JEFF W. M. BULTE**[1,2,4,5,*]

[1]Division of MR Research, Russell H. Morgan Department of Radiology and Radiological Science, The Johns Hopkins University School of Medicine, Baltimore, Maryland [2]Cellular Imaging Section and Vascular Biology Program, Institute for Cell Engineering, The Johns Hopkins University School of Medicine, Baltimore, Maryland [3]Q Therapeutics, Inc., 615 Arapeen Dr., Ste. 102, Salt Lake City, Utah [4]Department of Chemical and Biomolecular Engineering, The Johns Hopkins University School of Medicine, Baltimore, Maryland [5]Department of Biomedical Engineering, The Johns Hopkins University School of Medicine, Baltimore, Maryland

Abstract

Human glial precursor cells (hGPs) have potential for remyelinating lesions and are an attractive cell source for cell therapy of multiple sclerosis (MS). To investigate whether transplanted hGPs can affect the pathogenesis of experimental autoimmune encephalomyelitis (EAE), an animal model of MS, we evaluated the therapeutic effects of transplanted hGPs together with the *in vivo* fate of these cells using magnetic resonance imaging (MRI) and bioluminescence imaging (BLI). At 14 days post-EAE induction, mice ($n = 19$) were intracerebroventricularly (ICV) injected with 5×10^5 hGPs that were magnetically labeled with superparamagnetic iron oxide (SPIO) particles as MR contrast agent and transduced with firefly luciferase for BLI of cell survival. Control mice ($n = 18$) received phosphate buffered saline (PBS) vehicle only. The severity of EAE clinical disability in the hGP-transplanted group was significantly suppressed ($P < 0.05$) with concomitant inhibition of ConA and MOG-specific T cell proliferation in the spleen. Astrogliosis was reduced and a lower activity of macrophages and/or microglia was observed in the spinal cord ($P < 0.05$). On MRI, SPIO signal was detected within the lateral ventricle from 1 day post-transplantation and remained there for up to 34 days. BLI indicated that most cells did not survive beyond 5–10 days, consistent with the lack of detectable migration into the brain parenchyma and the histological presence of an abundance of apoptotic cells. Transplanted hGPs could not be detected in the spleen. We conclude that ICV transplantation of short-lived hGPs can have a remote therapeutic effect through immunomodulation from within the ventricle, without cells directly participating in remyelination.

Keywords

multiple sclerosis; EAE; glial precursor cells; MR imaging; bioluminescence imaging

*Correspondence to: Jeff W. M. Bulte, PhD, Department of Radiology and Institute for Cell Engineering, The Johns Hopkins University School of Medicine, 217 Traylor Bldg, 720 Rutland Ave, Baltimore, MD 21205-2195, USA. jwmbulte@mri.jhu.edu. Heechul Kim is currently at The Paik Institute for Clinical Research, Inje University, Busan 614-735, Republic of Korea

INTRODUCTION

Multiple sclerosis (MS) is an autoimmune disease of the central nervous system (CNS) and is characterized by multifocal inflammation, demyelination, and axonal and neuronal loss (Compston and Coles, 2008). MS affects predominantly young adults, and the progression of neurologic disability is typically characterized by a relapsing-remitting course (Hemmer et al., 2002). Although the etiology of MS remains unknown and the pathogenesis is obscure, it is generally thought to occur by the peripheral activation of autoreactive immune cells that, along with activated macrophages and/or microglia, attack the myelin components of CNS oligodendrocytes (Steinman, 2001). Remyelination by endogenous oligodendrocyte progenitor cells is limited in the demyelinated lesions of MS as axonal and neuronal damage progresses (Franklin and Ffrench-Constant, 2008). An analysis of the general pathology of MS has revealed two major potential therapeutic approaches, immunomodulation of T cell recruitment to the CNS and autoimmune T cell activation within peripheral lymphoid organs, and cell replacement for remyelination and the repair of demyelinated axons (Hemmer et al., 2002; Pluchino et al., 2003).

Although inflammatory activity toward the CNS is abrogated by immunomodulatory agents (Frohman et al., 2006), subsequent restoration of myelin is essential for recovery of neurologic function. Stem cells are immature cells that differentiate into multiple lineages and provide promising treatment strategies for several neurodegenerative diseases, including MS (Payne et al., 2008). In the animal model of MS, transplanted cells were shown to have the following positive effects on the pathogenesis of MS: (1) generation of oligodendrocytes (Pluchino et al., 2003) with capacity for remyelination (Hardison et al., 2006); (2) inhibition of T cell proliferation in the peripheral lymphoid organs (Einstein et al., 2007); (3) alteration of antigen-presenting cells (Pluchino et al., 2009); and (4) generation of anti-inflammatory cells to restore immune system balance (Takahashi et al., 2007). Although many multipotent stem cells have been developed and their functionality have been documented *in vitro* and/or *in vivo*, little is known about which cells are optimally suited for the treatment of MS. In addition, for therapeutic application in MS, the source of transplanted cells, and thus, their ability to adapt to the human system, must be considered, and they must be readily available to be tested experimentally in animal models of MS.

Recently, human glial precursor cells (hGPs) have been isolated and characterized (Campanelli et al., 2008; Sandrock et al., 2010; Windrem et al., 2004, 2008). These cells highly express glial precursor markers including A2B5, NG2, PDGFRa, and GFAP and express negligible levels of neuronal lineage markers (Campanelli et al., 2008). When hGPs were grafted into the brain of congenitally hypomyelinated neonatal shiverer mice, transplanted cells generated substantial myelin and prolonged survival rates (Walczak et al., 2011; Windrem et al., 2004, 2008), indicating the potential of hGPs for treatment of MS. To further evaluate the fate of grafted cells in neurological diseases such as MS, it is important to determine, noninvasively and in real time, where the transplanted cells affect the host environment and how long these cells survive following transplantation. In experimental auto-immune encephalomyelitis (EAE), an animal model of MS, transplanted neural stem cells have been monitored in the brain by magnetic resonance imaging (MRI) using superparamagnetic iron oxide (SPIO) labeling methods (Ben-Hur et al., 2007; Bulte et al., 2003; Muja et al., 2011; Politi et al., 2007). SPIO labeling does not affect survival and differentiation potential *in vitro* (Cohen et al., 2010), and labeled neural stem cells were found migrating along white matter tracts as demonstrated by MRI. MR cell tracking of SPIO-labeled cells is best suited for monitoring the delivery and initial distribution of cells as it does not provide information about cell survival, because of signal persistence after cell death and dilution of signal upon division of viable cells. Therefore, additional imaging modalities are needed to confirm the viability of transplanted cells (Muja and Bulte, 2009).

One such technique, bioluminescence imaging (BLI), uses luciferase-transduced transplanted cells that can be detected noninvasively *in vivo* by virtue of their reporter gene, which is expressed only when cells are alive (Berman et al., 2011; Li et al., 2008). In this study, using MRI and BLI side-by-side as complementary imaging techniques, we evaluated the effects of transplanted hGPs on EAE pathogenesis to determine their potential for therapy of MS.

MATERIALS AND METHODS

Cell Culture

Human GPs were isolated from human fetal forebrain (gestational age 20–23 weeks) and grown as described previously (Campanelli et al., 2008). After expansion, cells were cryopreserved for subsequent use. Human GPs were grown on poly-L-lysine- and laminin-coated dishes for 5 days *in vitro* before transplantation. Cells were grown in DMEM/F12 (Invitrogen, Carlsbad, CA) supplemented with 0.1% bovine serum albumin (Sigma, St. Louis, MO), 2% B27 supplementation (Invitrogen), 1% N2 supplementation (Invitrogen), 1% penicillin–streptomycin (Sigma), and basic fibroblast growth factor (20 ng/mL; Peprotech, Rocky Hill, NJ).

Chronic EAE Induction

All experiments were approved by our institutional Animal Care and Use Committee. Seven- to eight-week-old female C57BL/6 mice (Charles River, Frederick, MD) were immunized with a subcutaneous injection containing a mixture of 100 μL of 2.5 mg/mL $MOG_{35–55}$ peptide (NH2-MEVGWYRSPFSRVVHLYRNGK-COOH, Johns Hopkins Synthesis and Sequencing Facility, Department of Biological Chemistry, Baltimore, MD) emulsified with 100 μL incomplete Freund's adjuvant supplemented with *Mycobacterium tuberculosis* H37Ra (5 mg/mL, Difco, Detroit, MI). Mice were injected intraperitoneally (i.p.) with 300 ng of pertussis toxin (Biomol, Plymouth Meeting, PA) at the day of induction and 2 days later. After immunization, mice were observed daily for clinical signs of EAE. The progression of EAE was divided into seven clinical stages as follows: 0: asymptomatic; 1: partial loss of tail tonicity; 2: atonic tail; 3: hind leg weakness and/or difficulty in rolling over; 4: hind leg paralysis; 5: foreleg paralysis; and 6: death due to EAE.

Lentiviral Transduction and Magnetic Labeling of hGPs

hGPs were transduced for 24 h with a lentiviral vector carrying firefly luciferase gene (pLenti4-CMV-Luc). Stable expression of the firefly luciferase reporter gene was confirmed using bioluminescent imaging with an IVIS 200 system (Caliper LifeSciences, Hopkinton, MA). Post-lentiviral transduction, hGPs were incubated with iron oxide formulation Molday ION Rhodamine B (BioPal, Worcester, MA) 10 μg Fe/mL for 24 h. Before transplantation, cells were washed and suspended in 10 mM PBS, pH 7.4, at a density of $10^5\ \mu L^{-1}$.

Cell Transplantation

Transplantation of hGPs was performed on day 14 after EAE induction. Mice were anesthetized i.p. with ketamine (80 mg/kg) and xylazine (10 mg/kg). Labeled cells (5×10^5 in 5 μL sterile PBS) were stereotaxically injected into the right ventricle (from bregma, AP = 0 mm, ML = 1 mm, and DV = 2.5 mm) of 19 mice. Control EAE mice received an injection of PBS vehicle ($n = 18$). To prevent immunorejection of human cells, both mice cohorts received daily i.p. injections of 10 mg/kg cyclosporine A (LC Laboratories, Woburn, MA) throughout the experiment beginning 1 day before transplantation. To control for attenuating effects caused by immunosuppression, an additional cohort of mice ($n = 15$) that did not receive cyclosporine A was included.

In Vivo Optical Bioluminescence Imaging

Cellular bioluminescence was imaged using a Caliper LifeSciences IVIS 200 system. Isoflurane (1–2%)-anesthetized mice were injected i.p. with D-luciferin (150 mg/kg; Caliper LifeSciences) and imaged at 5-min intervals until peak bioluminescence signal was attained. The photon flux (photons per second) was calculated for the entire head region using LIVINGIMAGE software.

Serial *In Vivo* MRI

In vivo MRI was performed on individual mice at days 1, 5, 10, 20, and 34 PT using a Bruker 9.4-T horizontal bore spectrometer. Mice were anesthetized using 1–2% isoflurane and placed inside a 30 mm volume coil. Images were obtained using a two-dimensional fast low-angle shot (FLASH) sequence with the following parameters: repetition time (TR) = 316.5 ms; echo time (TE) = 3.5 ms; field of view (FOV) = 1.2 cm × 1.2 cm; resolution = 80 μm × 80 μm; number of averages = 6; slice thickness = 400 μm; number of slices = 30; and flip angle = 45°.

Tissue Harvesting

EAE animals were sacrificed at 10 ($n = 3$, each group), 20 ($n = 3$, each group), and 34 ($n = 12$ for control group and $n = 13$ for experimental group) days post-transplantation. Animals were deeply anesthetized using sodium pentobarbital, transcardially perfused with 4% paraformaldehyde (PFA) in 10 mM PBS (pH = 7.4), and their brains and spinal cords were removed and immersed in PFA for 24 h at 4°C.

T Cell Proliferation Assay

Proliferative responses were assayed as described previously (Matsumoto et al., 1996). Mice with average clinical scores from each group at days 10 and 20 PT were sacrificed ($n = 3$ per group). Spleens were excised immediately before PFA perfusion and then weighed. Splenic mononuclear cells (MNCs) were dissociated and suspended in culture medium containing Dulbecco's modified Eagle's medium (Invitrogen) supplemented with 1% (v/v) minimum essential medium (Invitrogen), 50 IU/mL penicillin, 50 mg/mL streptomycin, and 10% (v/v) fetal calf serum (Invitrogen). MNCs were isolated and incubated (2×10^5 MNCs with 100 μL of culture medium) in 96-well plates. $MOG_{35–55}$ (Johns Hopkins Synthesis and Sequencing Facility) and Concanavalin A (Con A; Sigma) were added at final concentrations of 10 μg/mL $MOG_{35–55}$ and 1 μg/mL Con A. After 72 h of incubation, cells were incubated for 4 h with 20 μL of CellTiter 96® AQueous Non-Radioactive Cell Proliferation Assay (Promega Corporation, Madison, WI), and the converted substance absorbance was read at 490 nm using a microplate reader (Beckman coulter, AD340).

Ex Vivo MRI

Fixed brain samples were immersed in aqueous perfluoropolyether (Fomblin, AUSIMONT USA, Thorofare, NJ) (Bulte et al., 1999), and *ex vivo* MR images were obtained using an 11.7-T Bruker NMR spectrometer and a 15 mm coil. Images were obtained using a three-dimensional (3D) FLASH sequence with the following parameters: TR = 150 ms; TE = 8 ms; FOV = 1.5 cm × 1.1 cm × 0.85 cm; resolution = 65 μm × 65 μm × 65 μm; flip angle = 30°; and number of averages = 2.

Histological Analysis

Following *ex vivo* MRI, tissues were transferred to 30% sucrose in PBS for cryoprotection, and serial 10-μm frozen sections were obtained for histological analysis. Transplanted hGPs were identified by Prussian blue staining, direct rhodamine fluorescence visualization, and immunostaining with anti-human nuclear antigen antibody (Millipore, Billerica, MA).

For Prussian blue staining, sections were reacted with 2% potassium ferrocyanide (Sigma) in 6% HCl for 30 min and with diaminobenzidine (DAB; 140 μg/mL; Sigma) for 15 min followed by another 15-min incubation with 0.03% H_2O_2-activated DAB, as described previously (Bulte et al., 2004). To examine inflammation, gliosis, myelination, and apoptosis in the spinal cord and brain, sections were immunostained using cell-type-specific markers: rat anti-mouse Mac3 (BD Biosciences, San Jose, CA) and biotinylated isolectin B4 (Sigma) for macrophages/activated microglia; rat anti-mouse CD45 (AbD Serotec, Raleigh, NC) for myeloid leukocytes; rabbit anti-glial fibrillary acidic protein (GFAP; Dako, Carpinteria, CA) for astrocytes; rat anti-MBP (AbD Serotec) for myelin; and rabbit anti-cleaved caspase-3 (c-caspase-3, Cell signaling Technology, Danvers, MA) for apoptotic cells.

For immunofluorescence staining, sections were incubated for 1 h with 10% normal goat serum and then with the primary antibodies overnight at 4°C. For secondary reaction, the sections were incubated with Alexa 488-conjugated goat anti-rabbit IgG or goat anti-mouse IgG (Invitrogen). For secondary reaction with Mac3 immunostaining, sections were first incubated with biotinylated anti-rat IgG (Vector Labs, Burlingame, CA) and then with streptavidin-conjugated FITC (Zymed, Invitrogen). Histochemical and immunofluorescent images were obtained using Olympus BX51 microscope with attached Olympus DP70 camera.

For semiquantitative analysis of immunoreactivity for Mac3 and GFAP in the spinal cord, the intensities of Mac3- and GFAP-positive immunofluorescence on the captured images of the dorsal columns and white matter were measured using the Adobe Photoshop Histogram command, as described previously (Zhang et al., 2004). For both Mac3 and GFAP staining, the fluorescence intensity in the cervical, thoracic, and lumbar spinal cords of experimental ($n = 5$) and control animals ($n = 5$) was compared at day 34 PT. For each animal, 10 spinal cords were analyzed.

Statistical Analysis

For each experiment, all values are reported as the mean ± SEM. All comparisons between the hGP-transplanted group versus control vehicle group were performed using a two-tailed standard Student's *t*-test. For multivariate analysis, a linear mixed effects model was used to compare the daily change of clinical score in the measure between the two groups. In all cases, $P < 0.05$ was considered statistically significant.

RESULTS

Luciferase Gene-Transduced hGPs Can Be Tracked *In Vitro* and *In Vivo*

To track the viability of hGPs using BLI, we introduced a lentiviral vector carrying the firefly luciferase gene. *In vitro*, the BLI signal could be detected only for transduced hGPs and only after supplementing the medium with D-luciferin in a cell-dose-dependent manner (Fig. 1A). The signal was linearly dependent on cell concentration (Fig. 1B). *In vivo*, BLI signal was detected in mice that were transplanted with transduced hGPs after injection with D-luciferin, but not in mice without luciferin administration or mice that received luciferin but hGPs that were not transduced (Fig. 1C). To confirm that the magnitude of BLI signal corresponded to the amount of transplanted cells, different numbers of transduced hGPs were inoculated ($n = 3$ for each group). The BLI signal was highest in the mice that received the highest number of transduced hGPs with a good correlation between the signal and transplanted cell number (Fig. 1D,E). The BLI signal decreased in all groups 1 day after transplantation (Fig. 1D,E). These data indicate that BLi can be used as a quantitative

measure of the number of live cells with an *in vivo* sensitivity of at least 3×10^4 cells, i.e., >5% of the total amount of injected cells.

Transplanted hGPs Promote Recovery of Neurological Function in EAE

EAE was induced in C57BL/6 mice by immunization with $MOG_{35–55}$ peptide, and the clinical score was evaluated daily in individual mice. Fourteen days after EAE induction, EAE mice were divided into experimental and control groups, with mean clinical scores equal for both groups, and then were transplanted with either hGPs or PBS as vehicle control into the right lateral ventricle of the cerebrum. After transplantation, mice were scored daily for clinical signs of EAE during a 34-day period. The clinical course of EAE was significantly ameliorated in animals that received hGPs (Fig. 2A). The cumulative clinical scores for 49 days reflect a statistically significant reduction in the EAE clinical score in the hGP-transplanted group compared with the two control groups (Fig. 2B). To evaluate the daily change of clinical scores among hGP-transplanted, vehicle control, and the immunosuppression control group, multivariate analysis was performed. The regression results showed that the daily change for the vehicle control group was 0.0017 ($P = 0.511$), which is not statistically different from zero, in stark contrast to the daily change of −0.035 ($P < 0.001$) for the hGP-transplanted group. The daily change for the immunosuppression control group was −0.0191783 ($P < 0.001$). When the hGP-transplanted and immunosuppression control groups were compared, there was a significant daily change for the cell-transplanted group with a value of −0.0160925 lower ($P < 0.001$).

Transplanted hGPs Inhibit Proliferation of Antigen- and Mitogen-Specific T Cells and Result in Spleen Weight Reduction

To investigate the mechanisms responsible for the improvement in neurological symptoms detected in mice that received hGPs, we sought to address whether transplanted hGPs affect the capacity of T cells to respond to antigen and mitogen. We collected spleens and evaluated the T cell response to $MOG_{35–55}$ and Con A from treated animals and control animal at days 10 and 20 PT. Immunization and resulting lymphocyte proliferation usually is associated with spleen weight increase. Indeed, we detected significant increases in spleen weight during the EAE symptomatic period compared with normal 9-week-old mice (92.9 ± 8.5 mg, $n = 5$). A notable, statistically significant difference in weight was observed between the two groups for both time points ($P < 0.05$ each). The mean spleen weight (milligram per mouse) for hGPs-transplanted mice was 147 ± 12.5 ($n = 3$) at day 10 PT and 126 ± 24.1 ($n = 3$) at day 20 PT. For control animals, these values were 275 ± 25.9 ($n = 3$) and 249 ± 20.5 ($n = 3$), respectively (Fig. 3A). At day 10 PT, in the hGP-transplanted mice, the proliferative response to $MOG_{35–55}$ and Con A was significantly inhibited compared with control mice ($P < 0.05$; Fig. 3B). In addition, at day 20 PT, inhibitory effects of transplanted hGPs on the proliferation of antigen- and mitogen-responsive cells could be detected (Fig. 3C), but no hGPs could be detected in the spleen.

Transplanted hGPs Attenuate Macrophage Activation and Astrogliosis in the Spinal Cord

Because of the behavioral improvement and the inhibition of antigen-specific proliferation by transplanted hGPs, we next sought to address whether transplanted hGPs might also affect inflammation in the spinal cord. Infiltration of inflammatory cells and the activation of macrophages and/or microglia in the cervical spinal cord dorsal columns are commonly encountered in EAE (Black et al., 2006; Jones et al., 2008). We therefore performed immunohistochemical analysis to compare macrophage and/or microglia activity within the dorsal column in cervical, thoracic, and lumbar spinal cords of experimental and control animals at day 34 PT. The intensity of Mac3 immunoreactivity in the dorsal column of hGP-transplanted mice (mean fluorescence intensity 25.79 ± 2.32) was significantly decreased compared with control animals (47.22 ± 4.53, $P < 0.05$) (Fig. 4A–C).

Astrogliosis has been described during the acute phase of EAE and was considered to be an indirect byproduct of neuroinflammation. We immunostained the cervical, thoracic, and lumbar spinal cords of both groups using anti-GFAP antibody and analyzed the fluorescence intensity in white matter. The intensity of GFAP immunoreactivity in the white matter of spinal cords from treated mice (mean fluorescence intensity 32.38 ± 1.33) was significantly decreased compared with control animals (41.67 ± 3.15, $P < 0.05$) (Fig. 4D–F).

Serial BLI of Transplanted hGPs

To examine noninvasively the survival of transplanted hGPs in the brain of EAE mice, ATP-dependent firefly luciferase activity within stably transduced hGPs was detected using an IVIS 200 imaging system. Initial detection of luciferase activity within the CNS was performed 1 day after transplantation. At this time point, there was an intense luciferase signal in the brain (mean ± SEM, $6.80 \times 10^5 \pm 5.55 \times 10^4$ photons per second). Five days post-transplantation, the signal intensity greatly decreased to <13% of the initial value ($8.94 \times 10^4 \pm 1.68 \times 10^4$ photons per second), suggesting massive cell death after CNS transplantation. At day 10 PT, the luciferase signal detected was ~ 5% of the initial signal ($3.76 \times 10^4 \pm 2.9 \times 10^3$ photons per second), and this signal was nearly absent at day 20 PT ($2.56 \times 10^4 \pm 1.43 \times 10^3$ photons per second) (Fig. 5). These data suggest that a minority of the transplanted hGPs survived beyond 10 days after transplantation, and that most of the transplanted cells had died at 20 days after transplantation.

Serial MRI of Transplanted hGPs

To examine noninvasively the location of transplanted SPIO-labeled hGPs, EAE mice were imaged on days 1, 5, 10, 20, and 34 PT using MRI. Serial *in vivo* MRI showed that on day 1 PT, hypointense signals were detected mainly within the ventricular system of the brain. On day 5 PT, the distribution of hypointense signals was similar to that seen at day 1 PT within the ventricle. This pattern of hypointense signal did not change on the MR images obtained on days 10, 20, and 34 PT (Fig. 6).

Ex vivo imaging was performed at 11.7 T for transplanted EAE mice at 10 ($n = 3$), 20 ($n = 3$), and 34 ($n = 13$) PT to confirm the location of the hypointensities observed *in vivo* and to detect potential extraventricular hGPs migration patterns at higher resolution. The primary distribution of hypointensities on days 10, 20, and 34 PT (Fig. 7) was within the ventricular system and, occasionally, in white matter tracts, in accordance to that observed in the *in vivo* imaging (Fig. 6).

Histological Analysis of Transplanted hGPs

To confirm that the hypointensities detected by MRI were due to labeled cells, we performed DAB-enhanced Prussian blue histochemistry to detect the iron oxide label. hGPs were detected in the ventricles on days 10 (Fig. 7B,C), 20 (Fig. 7E,F), and 34 (Fig. 7H,I) PT, and the distribution of Prussian blue stain was correlated with the distribution of hypointensities within MR images on days 10 (Fig. 7A), 20 (Fig. 7D), and 34 PT (Fig. 7G), respectively. As seen with MRI, histological analysis indicated that transplanted human GPs were retained within the cerebral ventricular system.

To confirm that the photon emission detected by BLI was due to live hGPs, we performed immunohistochemistry for human-specific nuclear antigen (HuNu) to detect cells of human origin. At day 10 PT, there were very few HuNu-positive cells in the lateral ventricle (arrowheads), and nuclear pyknosis (arrows) was detected in the rhodamine-positive cells (Molday ION Rhodamine B-labeled) (Fig. 8A–H). At day 20 PT, there were no HuNu-positive hGPs present in the ventricle, whereas rhodamine-positive Molday ION-labeled cells could be detected (Fig. 8I–L). In addition, rhodamine-positive cells retained the cell

membrane and demonstrated nuclear pyknosis (Fig. 8O–R, arrow). No evidence for myelination by transplanted human GPs was detected (data not shown).

To determine whether transplanted hGPs underwent apoptosis or were taken up by professional phagocytes, we performed immunohistochemistry with anti-c-caspase-3 for detection of apoptotic cells and with anti-CD45 and isolectin B4 for detection of immune cells. C-caspase-3 immunoreactivity was found to be co-localized with rhodamine-positive cells at days 10 and 20 PT (Fig. 9). At day 10 PT, CD45-positive cells infiltrated into the ventricle with some CD45-positive cells containing Molday ION Rhodamine B (Fig. 10A–D). At day 20 PT, most rhodamine-positive cells were co-localized with CD45 (Fig. 10E–H). Isolectin B4-positive macrophages also contained Molday ION Rhodamine B in the ventricle at days 10 and 20 PT (Fig. 11). Only a few Molday ION Rhodamine B-positive cells were detected in the parenchyma, which were isolectin B4-positive for macrophages.

DISCUSSION

The overall goal of this study was to evaluate the therapeutic efficacy and underlying cellular mechanisms of transplanted hGPs in EAE, an animal model of MS. This study focused on monitoring the location and survival of these cells in the brain using MRI and BLI and, in particular, on assessing the immunomodulatory effects of hGPs transplants as related to the pathogenesis of EAE.

In vivo tracking of transplanted cells can inform us about the fate and location of transplanted cells in real time. MRI provides high-resolution 3D images of the exact anatomical location of labeled transplanted cells in the brain (Ben-Hur et al., 2007; Bulte et al., 2003; Cohen et al., 2010; Muja et al., 2011). Because MRI has limitations in determining the viability of labeled transplanted cells, another imaging modality is required. We therefore combined MRI with BLI to simultaneously monitor the location and viability of transplanted cells *in vivo* within the same animal. Although we did not correlate BLI signal with the exact transplanted cell number, as this depends on the actual anatomical depth of their location, previous studies demonstrated that photon emission from luciferase-labeled cells was sufficient to detect $1–2.5 \times 10^3$ cells in the peritoneal cavity, 1×10^4 cells at subcutaneous sites, and 1×10^6 circulating cells (Edinger et al., 1999; Sweeney et al., 1999). We successfully monitored the survival of transplanted hGPs within the brain using serial *in vivo* BLI, and histochemical analysis confirmed that BLI findings did accurately reflect the viability of transplanted cells.

Although our end-point analysis was performed during the chronic EAE phase, characterized by recurrent pathological demyelination and remyelination, we transplanted hGPs during the end stage of the acute phase of EAE, i.e., during the period of inflammation. Our results demonstrate that even though transplanted hGPs do not participate in myelination and their survival is limited to about 10 days postgrafting, they are able to ameliorate the EAE clinical score within the first 10 days after transplantation. The effect of transplanted hGPs in EAE was associated with a reduced proliferation of antigen-reactive T cells in the peripheral lymphoid organs and a reduced activation of macrophage and/or microglia and astrocytes in the spinal cord lesions of EAE. These findings raise the question of how transplanted hGPs that reside within the cerebral ventricles can significantly decrease the proliferation of reactive T cells in the peripheral lymphoid organs of EAE. In an inflammatory condition, such as MS or EAE, inflammatory cells migrate into the CNS through the blood–brain barrier as well as through the blood–cerebrospinal fluid barrier of the choroid plexus (Engelhardt et al., 2001; Ransohoff et al., 2003). Because of its juxtaposition at the vascular and the ventricular system, where it filters metabolites and produces cerebrospinal fluid, the choroid plexus plays a critical role in maintaining CNS

homeostasis including the regulation of immune cell trafficking (Redzic et al., 2005). Large numbers of MHC class II(+) putative dendritic cells (DCs) and macrophages are located in the choroid plexus epithelium (McMenamin et al., 2003), and these cells play a role in antigen presentation (Polfliet et al., 2002). When DCs were injected into the ventricle of the brain in EAE, they migrated to both the CNS parenchyma and to the peripheral lymphoid organs, stimulated the antibody response against MOG, and affected EAE paralysis; animals that received DCs showed aggravated EAE clinical signs compared with EAE controls (Hatterer et al., 2008). The systemic delivery of neural stem/precursor cells inhibited the activation of myeloid DCs and restrained the expansion of antigen-specific encephalogenic T cells (Pluchino et al., 2009). Although this work did not detect migration of intracerebroventricularly (ICV)-transplanted cells into spleen and did not directly address potential interactions between DCs and hGPs, we cannot rule out the possibility that inhibition of the proliferation of antigen-specific encephalogenic T cells in the peripheral lymphoid organs and activation of macrophages and/or microglia in the CNS were mediated by DCs in the process of proliferation of MOG-specific T cells in the presence of transplanted hGPs. This process may have inhibited DC function in the ventricle, similar to antigen presentation in the brain parenchyma and peripheral lymphoid organs.

Another major question is why most transplanted hGPs are retained within the ventricles. Signals that are generated from the host can modulate the migration of transplanted hGPs, such as adhesion molecules and chemokines (Belmadani et al., 2006; Ben-Hur et al., 2007; Cheng et al., 2009; Ourednik et al., 2009; Rampon et al., 2008). In MS and EAE, chemokines and adhesion molecules can be released in the CNS, which can contribute to recruiting additional inflammatory cells to the CNS parenchyma (Engelhardt, 2008). Furthermore, in EAE, the expression of VCAM-1, ICAM-1, and Mad-CAM-1 was increased in the choroid plexus (Engelhardt et al., 2001). In our study, we detected that most transplanted hGPs were located adjacent to the choroid plexus as evidenced by DAB-enhanced Prussian blue stain and red fluorescence (rhodamine conjugated to the SPIO MR contrast agent) and HuNu-positive cells (Figs. 7 and 8). We detected that transplanted hGPs underwent cell death beyond 20 days post-ICV transplantation in EAE despite of immunosuppression with cyclosporine A. Although we did not confirm here that SPIO labeling for MRI does not adversely affect hGP cell viability and differentiation *in vitro,* the general consensus is such that SPIO labeling neither negatively impacts neural precursor cell viability and function (Cohen et al., 2010; Neri et al., 2008) nor interferes with immunomodulation of labeled stem cells in patients with amyotrophic lateral sclerosis and MS (Karussis et al., 2010).

One explanation for the poor viability of hGPs beyond 2 weeks is that the microenvironment of the cerebrospinal fluid in adult mice does not provide sufficient trophic support (Buddensiek et al., 2009). Indeed, we found that most transplanted hGPs remained restricted at the site of delivery (the lateral ventricle), i.e., the cerebrospinal fluid environment. The absence of hGP infiltration within the CNS parenchyma indicates that these cells were incapable of responding to migratory cues provided at sites of inflammation and or/ demyelination (Hinks and Franklin, 1999). This finding is in contrast to studies in developing brain and immunodeficient animals where ICV-transplanted glial precursor cells survived and migrated extensively. However, the migration process was relatively slow; at 14 days after transplantation, the number of migrating cells was negligible (Walczak et al., 2011). Extensive migration and proliferation of GPs has also been shown in the demyelinated and/or inflammatory lesions following transplantation directly into the lesion (Jin et al., 2011; Walczak et al., 2011). Furthermore, it has been reported that human embryonic stem-cell-derived oligodendrocyte progenitors transplanted directly into demyelinated lesions do not survive beyond 3 weeks within the mouse CNS, despite administration of immunosuppression to prevent xenograft rejection (Hatch et al., 2009). In

contrast, hESC-derived oligodendrocyte progenitors survived for more than 8 weeks after transplantation within rat CNS lesions (Keirstead et al., 2005). Together, the above studies indicate that the survival of xenografted cells is highly variable according to the animal species and/or trophic milieu at the site of transplantation and the immunosuppressive regimen used.

In summary, we show that ICV-transplanted hGPs ameliorate EAE paralysis by inhibiting the proliferation of antigen-specific T cells and the activation of macrophages and/or microglia in the CNS. Using a combination of two noninvasive imaging modalities, MRI and BLI, we demonstrated that most cells died by 5 days and remained located within the ventricle. Taken together with the prolonged (at least up to 50 days) improvement in therapeutic outcome, these results suggest that immunomodulation by hGPs is mediated by a remote effect.

Acknowledgments

The authors thank Jiangxia Wang, PhD (The Johns Hopkins Biostatistics Center, Bloomberg School of Public Health) for her advice regarding the statistical analysis and for performing multivariate analysis. They also thank Segun Bernard, Chulani Galpoththawela, and Michael Gorelik for technical assistance.

Grant sponsor: NIH; Grant numbers: 2RO1 NS045062, U54 CA151838; Grant sponsor: NMSS; Grant number: RG3630; Grant sponsor: Maryland Stem Cell Research Fund; Grant numbers: MSCRFII-0190, MSCRFII-0193.

References

Belmadani A, Tran PB, Ren D, Miller RJ. Chemokines regulate the migration of neural progenitors to sites of neuroinflammation. J Neurosci. 2006; 26:3182–3191. [PubMed: 16554469]

Ben-Hur T, van Heeswijk RB, Einstein O, Aharonowiz M, Xue R, Frost EE, Mori S, Reubinoff BE, Bulte JW. Serial in vivo MR tracking of magnetically labeled neural spheres transplanted in chronic EAE mice. Magn Reson Med. 2007; 57:164–171. [PubMed: 17191231]

Berman SC, Galpoththawela C, Gilad AA, Bulte JW, Walczak P. Long-term MR cell tracking of neural stem cells grafted in immunocompetent versus immunodeficient mice reveals distinct differences in contrast between live and dead cells. Magn Reson Med. 2011; 65:564–574. [PubMed: 20928883]

Black JA, Liu S, Hains BC, Saab CY, Waxman SG. Long-term protection of central axons with phenytoin in monophasic and chronic-relapsing EAE. Brain. 2006; 129:3196–3208. [PubMed: 16931536]

Buddensiek J, Dressel A, Kowalski M, Storch A, Sabolek M. Adult cerebrospinal fluid inhibits neurogenesis but facilitates gliogenesis from fetal rat neural stem cells. J Neurosci Res. 2009; 87:3054–3066. [PubMed: 19530161]

Bulte JW, Arbab AS, Douglas T, Frank JA. Preparation of magnetically labeled cells for cell tracking by magnetic resonance imaging. Methods Enzymol. 2004; 386:275–299. [PubMed: 15120257]

Bulte JW, Ben-Hur T, Miller BR, Mizrachi-Kol R, Einstein O, Reinhartz E, Zywicke HA, Douglas T, Frank JA. MR microscopy of magnetically labeled neurospheres transplanted into the Lewis EAE rat brain. Magn Reson Med. 2003; 50:201–205. [PubMed: 12815696]

Bulte JW, Zhang S, van Gelderen P, Herynek V, Jordan EK, Duncan ID, Frank JA. Neurotransplantation of magnetically labeled oligodendrocyte progenitors: Magnetic resonance tracking of cell migration and myelination. Proc Natl Acad Sci USA. 1999; 96:15256–15261. [PubMed: 10611372]

Campanelli JT, Sandrock RW, Wheatley W, Xue H, Zheng J, Liang F, Chesnut JD, Zhan M, Rao MS, Liu Y. Expression profiling of human glial precursors. BMC Dev Biol. 2008; 8:102. [PubMed: 18947415]

Cheng P, Gao ZQ, Liu YH, Xue YX. Platelet-derived growth factor BB promotes the migration of bone marrow-derived mesenchymal stem cells towards C6 glioma and up-regulates the expression of intracellular adhesion molecule-1. Neurosci Lett. 2009; 451:52–56. [PubMed: 19133316]

Cohen ME, Muja N, Fainstein N, Bulte JW, Ben-Hur T. Conserved fate and function of ferumoxides-labeled neural precursor cells in vitro and in vivo. J Neurosci Res. 2010; 88:936–944. [PubMed: 19885865]

Compston A, Coles A. Multiple sclerosis. Lancet. 2008; 372:1502–1517. [PubMed: 18970977]

Edinger M, Sweeney TJ, Tucker AA, Olomu AB, Negrin RS, Contag CH. Noninvasive assessment of tumor cell proliferation in animal models. Neoplasia. 1999; 1:303–310. [PubMed: 10935484]

Einstein O, Fainstein N, Vaknin I, Mizrachi-Kol R, Reihartz E, Grigoriadis N, Lavon I, Baniyash M, Lassmann H, Ben-Hur T. Neural precursors attenuate autoimmune encephalomyelitis by peripheral immunosuppression. Ann Neurol. 2007; 61:209–218. [PubMed: 17187374]

Engelhardt B. Immune cell entry into the central nervous system: Involvement of adhesion molecules and chemokines. J Neurol Sci. 2008; 274:23–26. [PubMed: 18573502]

Engelhardt B, Wolburg-Buchholz K, Wolburg H. Involvement of the choroid plexus in central nervous system inflammation. Microsc Res Tech. 2001; 52:112–129. [PubMed: 11135454]

Franklin RJ, Ffrench-Constant C. Remyelination in the CNS: From biology to therapy. Nat Rev Neurosci. 2008; 9:839–855. [PubMed: 18931697]

Frohman EM, Racke MK, Raine CS. Multiple sclerosis—The plaque and its pathogenesis. N Engl J Med. 2006; 354:942–955. [PubMed: 16510748]

Hardison JL, Nistor G, Gonzalez R, Keirstead HS, Lane TE. Transplantation of glial-committed progenitor cells into a viral model of multiple sclerosis induces remyelination in the absence of an attenuated inflammatory response. Exp Neurol. 2006; 197:420–429. [PubMed: 16297915]

Hatch MN, Schaumburg CS, Lane TE, Keirstead HS. Endogenous remyelination is induced by transplant rejection in a viral model of multiple sclerosis. J Neuroimmunol. 2009; 212:74–81. [PubMed: 19477025]

Hatterer E, Touret M, Belin MF, Honnorat J, Nataf S. Cerebrospinal fluid dendritic cells infiltrate the brain parenchyma and target the cervical lymph nodes under neuroinflammatory conditions. PLoS One. 2008; 3:e3321. [PubMed: 18830405]

Hemmer B, Archelos JJ, Hartung HP. New concepts in the immunopathogenesis of multiple sclerosis. Nat Rev Neurosci. 2002; 3:291–301. [PubMed: 11967559]

Hinks GL, Franklin RJ. Distinctive patterns of PDGF-A, FGF-2, IGF-I, and TGF-beta1 gene expression during remyelination of experimentally-induced spinal cord demyelination. Mol Cell Neurosci. 1999; 14:153–168. [PubMed: 10532806]

Jin Y, Neuhuber B, Singh A, Bouyer J, Lepore A, Bonner J, Himes T, Campanelli JT, Fischer I. Transplantation of human glial restricted progenitors and derived astrocytes into a contusion model of spinal cord injury. J Neurotrauma. 2011; 28:579–594. [PubMed: 21222572]

Jones MV, Nguyen TT, Deboy CA, Griffin JW, Whartenby KA, Kerr DA, Calabresi PA. Behavioral and pathological outcomes in MOG 35-55 experimental autoimmune encephalomyelitis. J Neuroimmunol. 2008; 199:83–93. [PubMed: 18582952]

Karussis D, Karageorgiou C, Vaknin-Dembinsky A, Gowda-Kurkalli B, Gomori JM, Kassis I, Bulte JW, Petrou P, Ben-Hur T, Abramsky O, Slavin S. Safety and immunological effects of mesenchymal stem cell transplantation in patients with multiple sclerosis and amyotrophic lateral sclerosis. Arch Neurol. 2010; 67:1187–1194. [PubMed: 20937945]

Keirstead HS, Nistor G, Bernal G, Totoiu M, Cloutier F, Sharp K, Steward O. Human embryonic stem cell-derived oligodendrocyte progenitor cell transplants remyelinate and restore locomotion after spinal cord injury. J Neurosci. 2005; 25:4694–4705. [PubMed: 15888645]

Li Z, Suzuki Y, Huang M, Cao F, Xie X, Connolly AJ, Yang PC, Wu JC. Comparison of reporter gene and iron particle labeling for tracking fate of human embryonic stem cells and differentiated endothelial cells in living subjects. Stem Cells. 2008; 26:864–873. [PubMed: 18218820]

Matsumoto Y, Abe S, Tsuchida M, Hirahara H, Abo T, Shin T, Tanuma N, Kojima T, Ishihara Y. Characterization of CD4-CD8− T cell receptor alpha beta + T cells appearing in the subarachnoid space of rats with autoimmune encephalomyelitis. Eur J Immunol. 1996; 26:1328–1334. [PubMed: 8647213]

McMenamin PG, Wealthall RJ, Deverall M, Cooper SJ, Griffin B. Macrophages and dendritic cells in the rat meninges and choroid plexus: Three-dimensional localisation by environmental scanning

electron microscopy and confocal microscopy. Cell Tissue Res. 2003; 313:259–269. [PubMed: 12920643]

Muja N, Bulte JWM. Magnetic resonance imaging of cells in experimental disease models. Prog Nucl Magn Reson Spectrosc. 2009; 55:61–77. [PubMed: 21552511]

Muja N, Cohen ME, Zhang JY, Kim H, Gilad AA, Walczak P, Ben-Hur T, Bulte JWM. Neural precursors exhibit distinctly different patterns of cell migration upon transplantation during either the acute or chronic phase of EAE: A serial MR imaging study. Magn Reson Med. 2011; 65:1738–1749. [PubMed: 21305597]

Neri M, Maderna C, Cavazzin C, Deidda-Vigoriti V, Politi LS, Scotti G, Marzola P, Sbarbati A, Vescovi AL, Gritti A. Efficient in vitro labeling of human neural precursor cells with superparamagnetic iron oxide particles: Relevance for in vivo cell tracking. Stem Cells. 2008; 26:505–516. [PubMed: 17975226]

Ourednik V, Ourednik J, Xu YF, Zhang Y, Lynch WP, Snyder EY, Schachner M. Cross-talk between stem cells and the dysfunctional brain is facilitated by manipulating the niche: Evidence from an adhesion molecule. Stem Cells. 2009; 27:2846–2856. [PubMed: 19785036]

Payne N, Siatskas C, Bernard CCA. The promise of stem cell and regenerative therapies for multiple sclerosis. J Autoimmun. 2008; 31:288–294. [PubMed: 18504116]

Pluchino S, Quattrini A, Brambilla E, Gritti A, Salani G, Dina G, Galli R, Del Carro U, Amadio S, Bergami A, Furlan R, Comi G, Vescovi AL, Martino G. Injection of adult neurospheres induces recovery in a chronic model of multiple sclerosis. Nature. 2003; 422:688–694. [PubMed: 12700753]

Pluchino S, Zanotti L, Brambilla E, Rovere-Querini P, Capobianco A, Alfaro-Cervello C, Salani G, Cossetti C, Borsellino G, Battistini L, Ponzoni M, Doglioni C, Garcia-Verdugo JM, Comi G, Manfredi AA, Martino G. Immune regulatory neural stem/precursor cells protect from central nervous system autoimmunity by restraining dendritic cell function. PLoS One. 2009; 4:e5959. [PubMed: 19543526]

Polfliet MMJ, van de Veerdonk F, Dopp EA, van Kesteren-Hendrikx EML, van Rooijen N, Dijkstra CD, van den Berg TK. The role of perivascular and meningeal macrophages in experimental allergic encephalomyelitis. J Neuroimmunol. 2002; 122:1–8. [PubMed: 11777538]

Politi LS, Bacigaluppi M, Brambilla E, Cadioli M, Falini A, Comi G, Scotti G, Martino G, Pluchino S. Magnetic-resonance-based tracking and quantification of intravenously injected neural stem cell accumulation in the brains of mice with experimental multiple sclerosis. Stem Cells. 2007; 25:2583–2592. [PubMed: 17600110]

Rampon C, Weiss N, Deboux C, Chaverot N, Miller F, Buchet D, Tricoire-Leignel H, Cazaubon S, Evercooren ABV, Couraud PO. Molecular mechanism of systemic delivery of neural precursor cells to the brain: Assembly of brain endothelial apical cups and control of transmigration by CD44. Stem Cells. 2008; 26:1673–1682. [PubMed: 18450824]

Ransohoff RM, Kivisakk P, Kidd G. Three or more routes for leukocyte migration into the central nervous system. Nat Rev Immunol. 2003; 3:569–581. [PubMed: 12876559]

Redzic ZB, Preston JE, Duncan JA, Chodobski A, Szmydynger-Chodobska J. The choroid plexus-cerebrospinal fluid system: From development to aging. Curr Top Dev Biol. 2005; 71:1–52. [PubMed: 16344101]

Sandrock RW, Wheatley W, Levinthal C, Lawson J, Hashimoto B, Rao M, Campanelli JT. Isolation, characterization and preclinical development of human glial-restricted progenitor cells for treatment of neurological disorders. Regen Med. 2010; 5:381–394. [PubMed: 20455649]

Steinman L. Multiple sclerosis: A two-stage disease. Nat Immunol. 2001; 2:762–764. [PubMed: 11526378]

Sweeney TJ, Mailander V, Tucker AA, Olomu AB, Zhang W, Cao Y, Negrin RS, Contag CH. Visualizing the kinetics of tumor-cell clearance in living animals. Proc Natl Acad Sci USA. 1999; 96:12044–12049. [PubMed: 10518573]

Takahashi K, Prinz M, Stagi M, Chechneva O, Neumann H. TREM2-transduced myeloid precursors mediate nervous tissue debris clearance and facilitate recovery in an animal model of multiple sclerosis. PLoS Med. 2007; 4:e124. [PubMed: 17425404]

Walczak P, All AH, Rumpal N, Gorelik M, Kim H, Maybhate A, Agrawal G, Campanelli JT, Gilad AA, Kerr DA, Bulte JW. Human glial-restricted progenitors survive, proliferate, and preserve electrophysiological function in rats with focal inflammatory spinal cord demyelination. Glia. 2011; 59:499–510. [PubMed: 21264955]

Windrem MS, Nunes MC, Rashbaum WK, Schwartz TH, Goodman RA, McKhann G II, Roy NS, Goldman SA. Fetal and adult human oligodendrocyte progenitor cell isolates myelinate the congenitally dysmyelinated brain. Nat Med. 2004; 10:93–97. [PubMed: 14702638]

Windrem MS, Schanz SJ, Guo M, Tian GF, Washco V, Stanwood N, Rasband M, Roy NS, Nedergaard M, Havton LA, Wang S, Goldman SA. Neonatal chimerization with human glial progenitor cells can both remyelinate and rescue the otherwise lethally hypomyelinated shiverer mouse. Cell Stem Cell. 2008; 2:553–565. [PubMed: 18522848]

Zhang Y, Huang P, Du G, Kanaho Y, Frohman MA, Tsirka SE. Increased expression of two phospholipase D isoforms during experimentally induced hippocampal mossy fiber outgrowth. Glia. 2004; 46:74–83. [PubMed: 14999815]

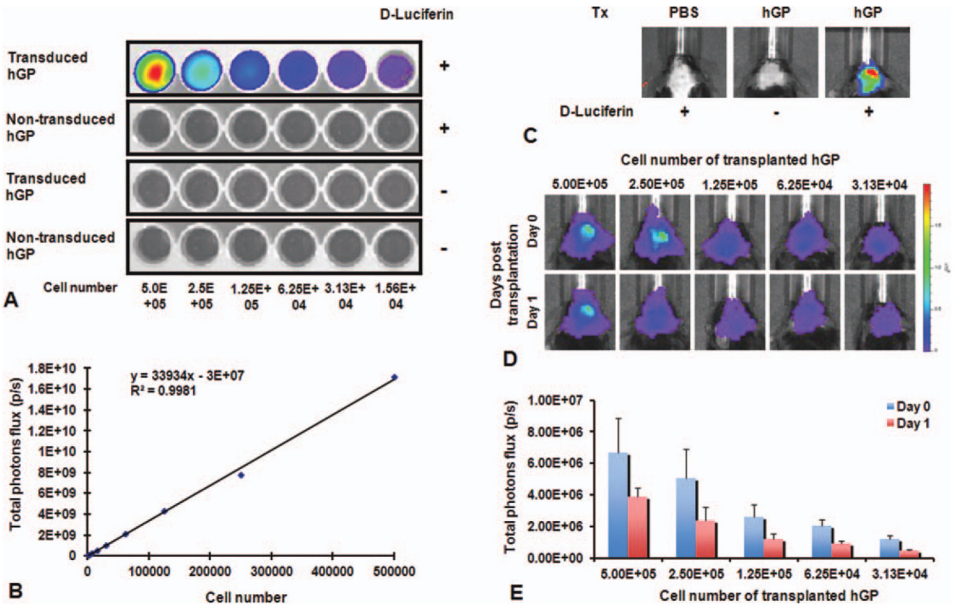

Fig. 1.

In vitro and *in vivo* characterization of luciferase gene-transduced hGPs. (**A**) *In vitro* BLI of transduced hGP shows an increasing luciferase activity with increasing cell number. (**B**) Data were obtained in triplicate, showing a linear correlation between BLI signal and cell concentration (R^2 = 0.99). Each point represents the mean value ± SEM. (**C**) *In vivo* BL images following transplantation of transduced hGPs show signal only for transduced cells and luciferin administration. (**D** and **E**) An *in vivo* cell dilution curve was obtained allowing the correlation of BLI signal to the total cell number, with the BLI signal decreasing at day 1 after transplantation. Each point represents the mean value ± SEM. [Color figure can be viewed in the online issue, which is available at wileyonlinelibrary.com.]

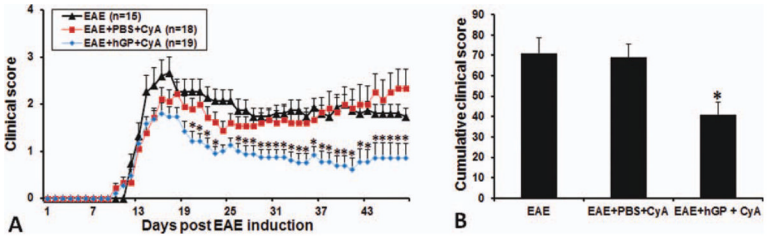

Fig. 2.

Therapeutic efficacy of transplanted hGPs. (**A**) Clinical scoring of EAE. The average scores in the hGP-transplanted group (blue diamonds) are significantly decreased compared with the control groups with (red squares) or without (black triangles) cyclosporine A treatment. (**B**) Cumulative mean clinical scores for all animals in the three groups over the 49-day period. The mean value for the hGP-transplanted group is significantly lower compared with the two control groups (*$P < 0.05$). [Color figure can be viewed in the online issue, which is available at wileyonlinelibrary.com.]

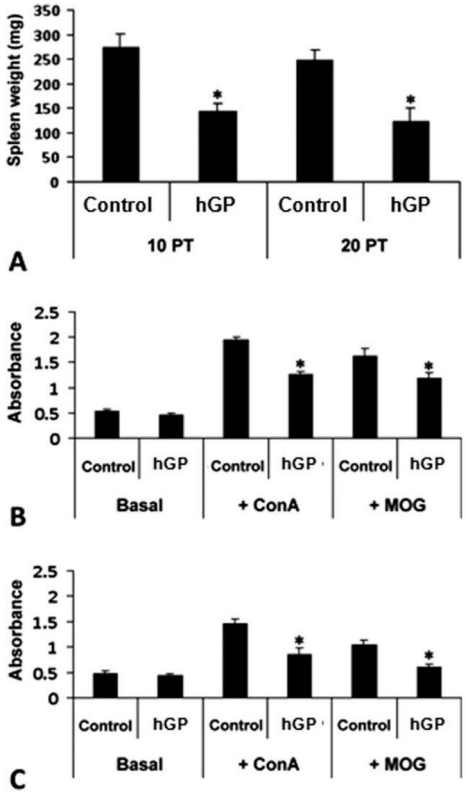

Fig. 3.

Immunomodulation of EAE mice transplanted with hGPs vs. vehicle control. Spleens were dissociated from EAE mice at days 10 and 20 PT, weighed, and cultured as single-cell suspensions. (**A**) Spleen weight was reduced after transplantation of hGPs. (**B** and **C**) When compared with native proliferation (i.e., without MOG and ConA stimulation), transplanted hGPs significantly attenuated the proliferation of immunostimulated (+ConA) and antigen-reactive (+MOG) T cells at days 10 (B) and 20 (C) PT (*$P < 0.05$).

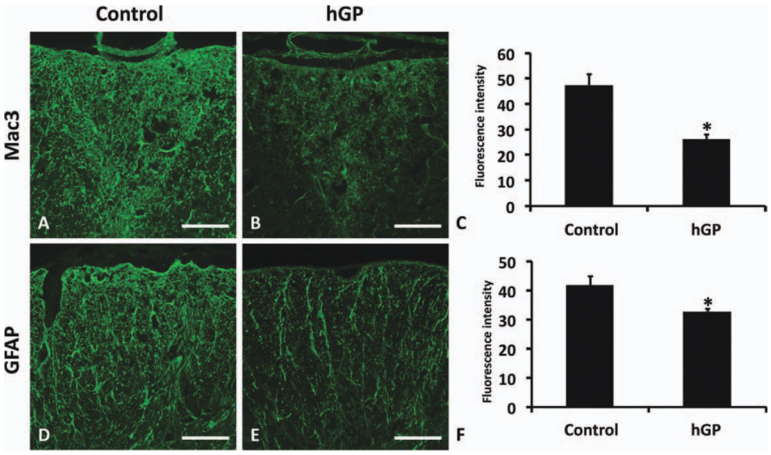

Fig. 4.

Transplanted hGPs reduce inflammation and astrogliosis in EAE. Representative images of immunostaining for Mac3 (**A** and **B**) and GFAP (**D** and **E**) in the spinal cord of hGP-transplanted (B and E) and control animals (A and D). Semiquantitative analysis of Mac3 (**C**) and GFAP (**F**) immunoreactivity in the dorsal column and white matter, respectively. Transplanted hGPs significantly attenuated Mac3 and GFAP immunoreactivity in the dorsal column and in the white matter of the spinal cord, respectively (*$P < 0.05$). Data are means ± SEM of intensity of immunofluorescence. Scale bar in A, B, D, and E = 100 μm. [Color figure can be viewed in the online issue, which is available at wileyonlinelibrary.com.]

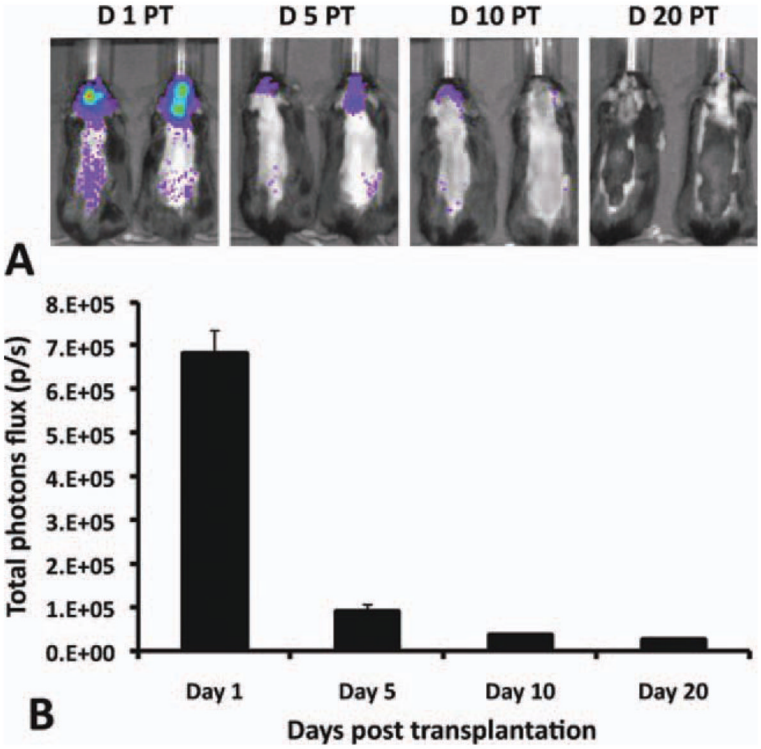

Fig. 5.

In vivo BLI of hGPs following ICV delivery at day 14 post-EAE induction. (**A**) Representative scans at days 1 ($n = 10$), 5, ($n = 9$), 10 ($n = 8$), and 20 ($n = 5$) PT. Color bar indicates intensity level of luciferase. (**B**) Luciferase intensity analysis over 20 days. Each point represents the mean value ± SEM. [Color figure can be viewed in the online issue, which is available at wileyonlinelibrary.com.]

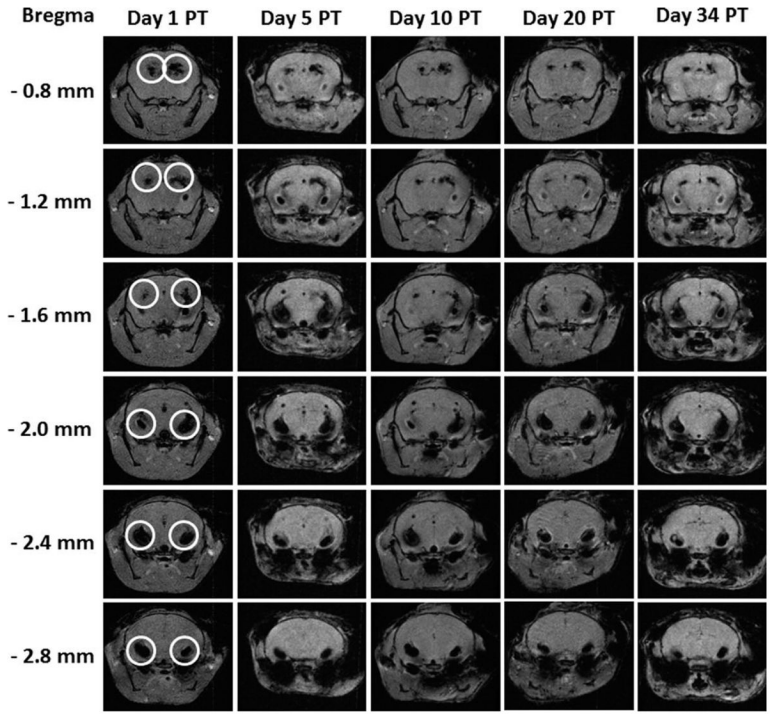

Fig. 6.

Serial *in vivo* MRI tracking of ICV-transplanted hGPs. SPIO-labeled hGPs were transplanted into the right ventricle of EAE mice. At day 1 after ICV transplantation, cells containing hypointense MRI signal (circled areas) were found in most of the ventricles, including both sides of the lateral ventricles. At 5, 10, 20, and 34 days PT, most cells were restricted within the ventricles. Coronal images were taken at the position of bregma from −0.8 to −2.4 mm.

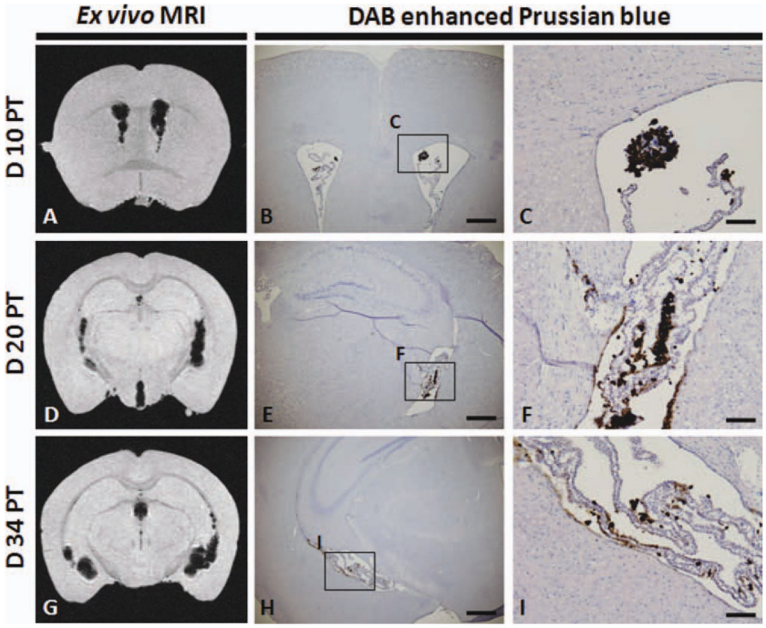

Fig. 7.

Correlation between MRI and histology. *Ex vivo* MR images were obtained at days 10 (**A**), 20 (**D**), and 34 (**G**) PT. DAB-enhanced Prussian blue histochemistry of the corresponding coronal brain section of the MRI on days 10 (**B** and **C**), 20 (**E** and **F**), and 34 (**H** and **I**) PT. C, F, and I are high-magnification images of the respective boxes in B, E, and H. Scale bar = 500 μm in B, E, and H and 100 μm in C, F, and I. [Color figure can be viewed in the online issue, which is available at wileyonlinelibrary.com.]

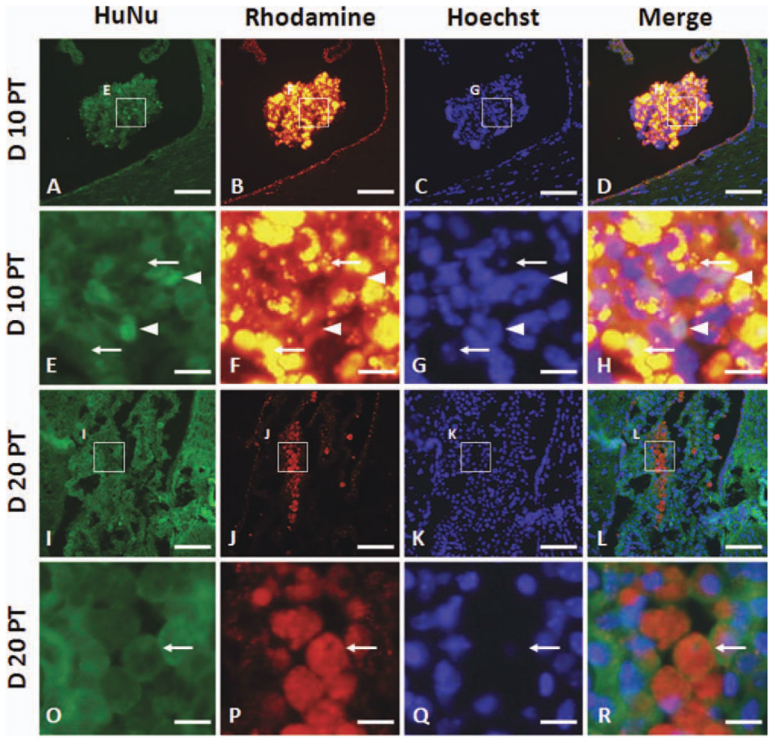

Fig. 8.

Histology of cell survival in the ventricles on days 10 (**A**–**H**) and 20 (**I**–**R**) PT. Sections were immunostained with human-specific nuclear antigen (HuNu) antibody (A, E, I, and O). Molday ION Rhodamine B-labeled hGPs are shown in panels B, F, J, and P. Sections were counterstained with Hoechst. The images in rows E–H and O–R are high-magnification images of the insets in the rows above. Scale bar = 60 μm in A–D and I–L and 10 μm in E–H and O–R. [Color figure can be viewed in the online issue, which is available at wileyonlinelibrary.com.]

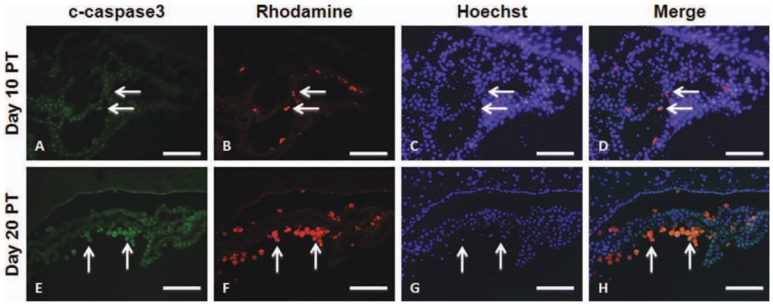

Fig. 9.

Immunohistochemistry of c-caspase-3 in mice that received Molday ION Rhodamine B-labeled hGPs on days 10 (**A**–**D**) and 20 (**EH**) PT. Sections were immunostained with anti-c-caspase-3 (A and E). Molday ION Rhodamine B-labeled hGPs are shown in panels B and F. The merged images, counterstained with Hoechst, are shown in panels D and H. Scale bar = 100 μm. [Color figure can be viewed in the online issue, which is available at wileyonlinelibrary.com.]

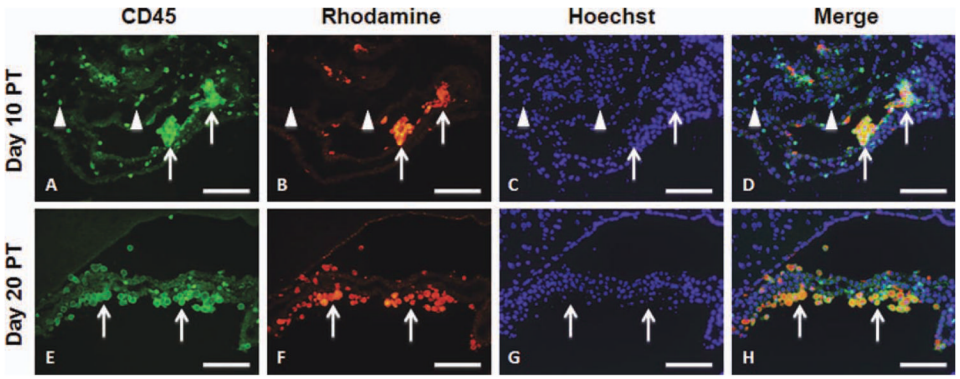

Fig. 10.

Immunohistochemistry of CD45 in mice that received Mol-day ION Rhodamine B-labeled hGPs on days 10 (**A**–**D**) and 20 (**E**–**H**) PT. Sections were immunostained with anti-CD45 (A and E). Molday ION Rhodamine B-labeled hGPs are shown in panels B and F. The merged images, counterstained with Hoechst, are shown in panels D and H. Scale bar = 100 μm. [Color figure can be viewed in the online issue, which is available at wileyonlinelibrary.com.]

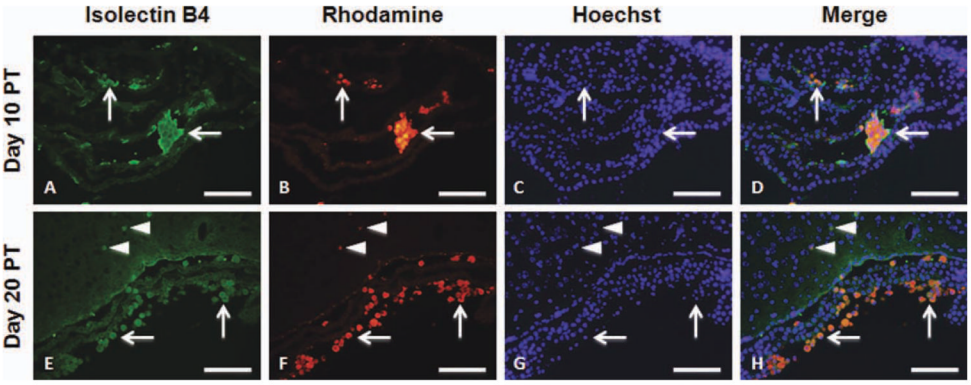

Fig. 11.

Immunohistochemistry of isolectin B4 in mice that received Molday ION Rhodamine B-labeled hGPs on days 10 (**A**–**D**) and 20 (**EH**) PT. Sections were immunostained with isolectin B4 (A and E). Mol-day ION Rhodamine B-labeled hGPs are shown in panels B and F. The merged images, counterstained with Hoechst, are shown in panels D and H. Scale bar = 100 μm. [Color figure can be viewed in the online issue, which is available at wileyonlinelibrary.com.]